Spin stripe order and superconductivity in layered transition metal oxides

Hans-Henning Klauss

Institut für Metallphysik und Nukleare Festkörperphysik, TU Braunschweig, D-38106 Braunschweig, Germany

E-mail: h.klauss@tu-bs.de

Abstract

In this work we present μSR experiments to examine spin stripe order in layered nickelate and cuprate systems. We discuss the signature of static spin stripe order in a zero field (ZF) μSR experiment. In the nickelate $La_{1.67}Sr_{0.33}NiO_4$ well separated signals from the antiferromagnetic (AF) domains and the domain walls are identified, whereas in Nd and Eu doped $La_{2-x}Sr_xCuO_4$ one asymmetrically broadened line is found. In both systems we observe slow fluctuations of the charge stripes. By changing the rare-earth and Sr doping levels in $La_{2-x-y}RE_ySr_xCuO_4$ we prove the strong correlation of static spin stripe order with the structural distortion in the low temperature tetragonal (LTT) phase, and demonstrate the competition of static spin stripe order with bulk superconductivity. Finally, evidence for a similar magnetic inhomogeneity in the electron doped high-T_C cuprate $Pr_{2-x}Ce_xCuO_4$ is presented.

(Some figures in this article are in colour only in the electronic version)

1. Introduction

Combined charge and spin ordering phenomena in doped transition metal oxides have attracted much attention due to their interplay with superconductivity in cuprates and giant magnetoresistance in manganites. Intense research has shown that periodic modulations of the charge density are a generic feature of doped transition metal oxides, such as cuprates, nickelates and manganites [1–6]. In terms of their electronic properties these systems are located in the intermediate regime between insulating antiferromagnets and metallic Fermi-liquid phases. In this situation the competition between the kinetic energy and the Coulomb repulsion between electrons may favour the formation of one-dimensional charge modulations described as charge stripe order or charge density waves in the strong and weak coupling limits, respectively. Due to the coupling of charge and spin degrees of freedom, static charge order results in an inhomogeneous distribution of spins with the same symmetry, and the
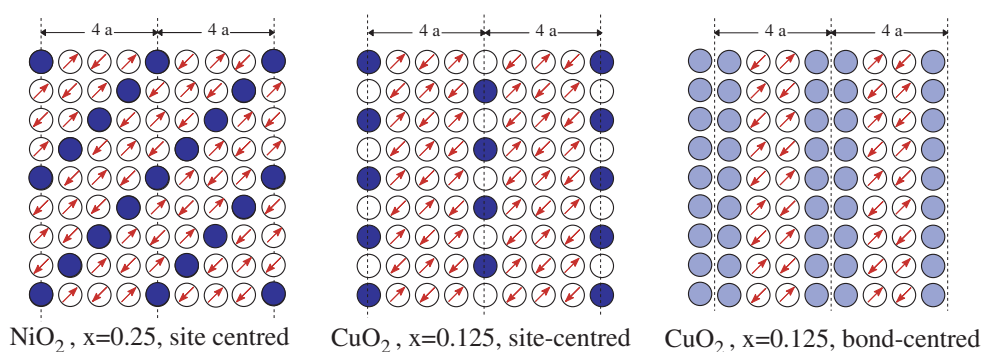
Figure 1. Examples of combined static charge and spin stripe order in the NiO_2 and CuO_2 planes [1] for specific charge doping levels x. Only the metal sites are shown. Filled circles indicate locations of holes (1 per site), arrows the orientation of ordered magnetic moments. In $La_{2-x}Sr_xNiO_4$ the stripes are oriented diagonal with respect to the crystallographic a–b-axes. In $La_{2-x-y}RE_ySr_xCuO_4$ they are oriented vertical and horizontal alternating from plane to plane. For cuprates, also the bond-centred stripe order is shown (shaded circles indicate a 1/4 hole density per site).

magnetic interaction of the spins eventually leads to magnetically long-range ordered phases. Combined charge and spin stripe order was predicted in numerical studies of the 2D single-band Hubbard model by Zaanen and Gunnarsson [7], and confirmed by many other theoretical studies (see e.g. the review by Carlson *et al* [10]). The detection of spin stripe order in nickelates and cuprates by neutron and synchrotron scattering gave the first experimental evidence for the occurrence of stripes in transition metal oxides [1, 12, 13]. The spin stripes consist of nearly undoped antiferromagnetic (AF) domains which are in one dimension only a few lattice constants wide. They are separated by non-magnetic charge stripes forming antiphase domain walls between the spin stripes. Examples are shown in figure 1. For the cuprates, recent inelastic neutron scattering results point to bond-centred stripes where the holes are delocalized over four Cu sites with an average hole density of 1/4, and the spin system can be regarded as an isotropic two-leg spin ladder [14]. The measured spin fluctuations are similar to those in superconducting cuprates, suggesting that charge inhomogeneity may be crucial for the mechanism of high temperature superconductivity. For recent reviews see e.g. [8–11].

In this work we present μSR experiments to examine spin stripe order in layered nickelate and cuprate systems. In $La_{2-x}Sr_xNiO_4$ the experimental evidence for static spin stripe order is very well established, and it serves as a reference system to discuss a specific signature of spin stripe order in a μSR experiment. In $La_{1.67}Sr_{0.33}NiO_4$ well separated signals from the AF domains and the domain walls are identified. In Nd and Eu doped $La_{2-x}Sr_xCuO_4$ we present systematic doping studies to prove the strong correlation of static spin stripe order with the structural distortion in the low temperature tetragonal (LTT) phase, and demonstrate the competition of static spin stripe order with bulk superconductivity in a wide range of charge carrier doping. In both systems we observe slow fluctuations of the stripe liquid. Finally, evidence for a similar magnetic inhomogeneity in the electron doped high-T_C cuprate $Pr_{2-x}Ce_xCuO_4$ is presented.

The paper is organized as follows. In the next section we describe how static magnetic order in nickelates and cuprates is detected in a μSR experiment. In section 3 the results on $La_{2-x}Sr_xNiO_4$ are presented. Section 4 is devoted to results on rare-earth doped $La_{2-x}Sr_xCuO_4$. It begins with a description of typical zero field spectra in a spin stripe ordered cuprate followed by the presentation of the resulting phase diagrams and a closer look
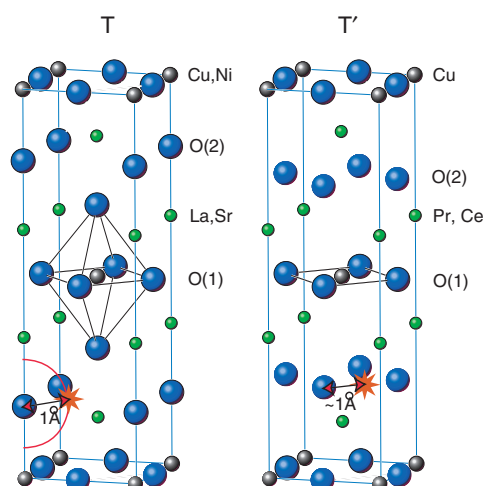
Figure 2. The basic tetragonal crystal structure T of $La_{2-x}Sr_xNiO_4$ and $La_{2-x}Sr_xCuO_4$ and T′ of $Pr_{2-x}Ce_xCuO_4$. The site of an implanted muon deduced from localized dipole calculations of the magnetic hyperfine coupling is indicated as a star. The muon forms a hydrogen-like bond with the oxygen O(2) with a bond length of ≈ 1 Å.

at the interplay of stripe order with superconductivity in the LTT phase. Section 5 describes experiments in the magnetically long-range ordered phase of $Pr_{2-x}Ce_xCuO_4$.

2. Muons—a local view on magnetic order in transition metal oxides

Local probe experiments like NMR [15–19], EPR [20] and μSR have contributed to the characterization of the static and dynamic properties of charge and spin stripe order in transition metal oxides. In these techniques an integrated signal over an ensemble of probes distributed in the sample volume is measured. Therefore one can get direct evidence about the inhomogeneity of the local environment of the probes, evaluate volume fractions of different phases, quantify the degree of inhomogeneity, and study the spin and charge dynamics on different timescales.

The positive muon with $S = 1/2$ provides a purely magnetic probe. In the transition metal oxides considered here the muon is located on interstitial sites forming a hydrogen-like covalent bond with oxygen ions. The site is of low crystallographic symmetry and a static electronic spin system gives rise to a finite local magnetic field B_{loc} at the muon site. The dominant magnetic interaction is dipole interaction with the electronic magnetic moments. Due to its $1/r^3$ dependence not only the nearest neighbour magnetic moments but also magnetic moments in distances up to several lattice constants contribute considerably, and the absolute value of B_{loc} depends on the spin structure. In addition the Fermi contact interaction with a spin-polarized electronic charge density at the muon site can contribute to B_{loc}. Whereas electronic structure calculations for $La_{2-x}Sr_xCuO_4$ on Hartree–Fock level suggest that this contribution is ≈ 100 times smaller than the dipole field [21], density functional calculations reveal indeed a considerable electron spin density transfer to the oxygen and subsequently to the muon sites [22]. The resulting Fermi contact field strength can be of similar size to, or even stronger than, the dipole field. Therefore a muon site determination based mainly on localized dipole field calculations in these materials may lead to wrong conjectures.

In the quasi-2D cuprates and nickelates a quantitative evaluation of the dipole and Fermi contact hyperfine coupling constants, e.g. by Knight shift experiments in the paramagnetic
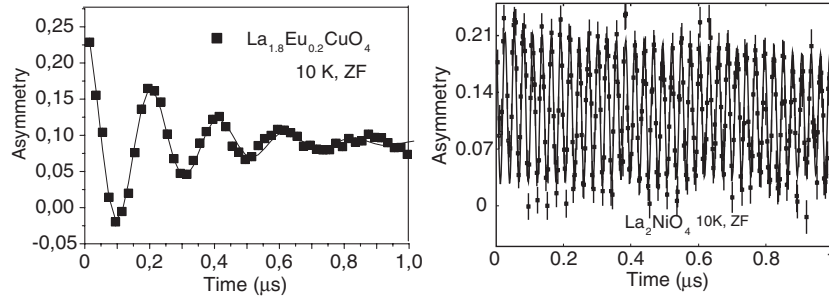
Figure 3. Typical zero field (ZF) μSR spectrum of undoped La$_{1.8}$Eu$_{0.20}$CuO$_4$ and La$_2$NiO$_4$ in the long-range AF ordered phase at 10 K.

state [23], has not been performed. The strong AF in-plane spin correlations suppress the magnetic susceptibility, and the observed Knight shift is nearly zero. Therefore a determination of the relative size of static magnetic moments at the Ni or Cu site from the measurement of B_{loc} is done by comparison with a calibration experiment performed on the undoped compound. The local field B_{loc} is measured via the muon spin precession frequency $\nu_\mu = 13.55\,\text{MHz/kG} \cdot B_{loc}$. In La$_2CuO_4$ one finds in the AF long-range ordered phase $\nu_\mu \approx 5.9$ MHz [24] at $T \ll T_N$ associated with an ordered Cu moment of 0.5 μ_B. Figure 3 shows a typical μSR time spectrum for La$_{1.8}$Eu$_{0.20}$CuO$_4$ at 10 K (left-hand panel). A single muon spin precession frequency of 4.9 MHz is deduced from a fit of the muon spin rotation signal. This frequency is $\approx$17% smaller than in La$_2$CuO$_4$ since a slightly different lattice structure ($Pccn$ instead of LTO; see section 4) gives rise to a modified hyperfine coupling strength. The precession signal is damped due to a distribution of the local field. This is caused mainly by the lattice inhomogeneity introduced by the Eu doping on the La site. The right-hand panel shows a μSR time spectrum for undoped La$_2$NiO$_4$ revealing a precession frequency of 36 MHz and a much smaller static line width.

A static local field at the muon site may also result from short-range spin correlations. Therefore spin order on a nanometre length scale like the short-range ordered phase (often called cluster spin glass, CSG) in lightly doped La$_{2-x}$Sr$_x$CuO$_4$ [25] and spin stripe order are detected with the same sensitivity as long-range ordered phases. For spin stripe ordered phases one may expect either a broad local field distribution or several distinct signals for the different local environments of the implanted muons.

The μSR technique cannot directly detect low frequency charge dynamics and charge order. Nevertheless, through the coupling of spin and charge degrees of freedom in these systems, mobile charge carriers modify the static and dynamic properties of the spin system which can be observed in μSR experiments [24].

In type-II superconductors, μSR in an external magnetic field applied transverse to the initial muon spin orientation (TF-μSR) is an important tool for determining the magnetic penetration depth λ and the static and dynamic properties of the flux line lattice in the Shubnikov phase [26, 27].

3. Spin stripe order in La$_{2-x}$Sr$_x$NiO$_4$

In La$_2$NiO$_4$ the nickel ions are in the Ni(II) 3d^8 high spin configuration ($S = 1$). Both t$_{2g}$ orbitals 3d$_{x^2-y^2}$ and 3d$_{3z^2-r^2}$ are singly occupied. Like La$_2$CuO$_4$ it is a Mott insulator with an AF ordered ground state below $T_N \approx 350$ K [28, 29]. Hole doping can be achieved by intercalation of excess oxygen or via the substitution of La^{3+} by Sr^{2+} in the
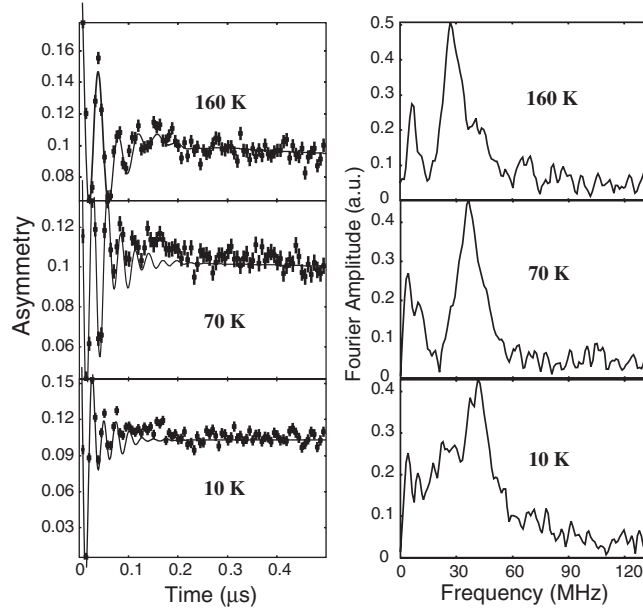
Figure 4. Zero field μSR time and frequency spectra of La$_{1.66}$Sr$_{0.33}$NiO$_4$ at various temperatures with the initial muon spin orientation parallel to [110] [39].

series La$_{2-x}$Sr$_x$NiO$_4$. An enhanced conductivity is found only for doping beyond $x = 0.6$. Metallic behaviour with positive dρ/dT is found only for $x > 1$, and no superconductivity is observed [30].

3.1. Undoped La$_2$NiO$_4$

μSR experiments on a single crystal of La$_2$NiO$_4$ reveal a spontaneous muon spin precession frequency of $\approx$36 MHz at 10 K in the long-range Néel ordered state (see figure 3, right-hand panel) in good agreement with earlier work on polycrystals [34]. Note the very slow relaxation of the spin precession reflecting the homogeneity of the long-range AF order.

The precession frequency is $\approx$6 times larger than the low temperature saturation value found in La$_2$CuO$_4$. This difference cannot be explained by the slightly larger value of the ordered moment of $\mu_{Ni} \approx 0.8 \ \mu_B$ [36, 37] instead of $\mu_{Cu} \approx 0.5 \ \mu_B$. Assuming pure dipole interaction, Jestaedt *et al* [38] concluded a muon site in the NiO$_2$ planes close to the centre of a Ni$_4$ plaquette. Alternatively an increased spin-polarization at the apical oxygen O(2) may also lead to a strongly enhanced local field at a muon bound to this oxygen. ^{139}La-NMR in La$_2$CuO$_4$ [40] and La$_2$NiO$_4$ [19, 41] reveal an 18 times larger magnetic hyperfine coupling in the nickelate due to the superexchange via the apical oxygen. The increased spin-polarization at the apical oxygen O(2) is explained qualitatively by the much larger overlap of the O(2) 2p$_z$ orbital with the transition metal 3d$_{3z^2-r^2}$ orbital which is spin-polarized only in the nickelate.

3.2. Spin stripes in La$_{1.67}$Sr$_{0.33}$NiO$_4$

Linear charge and spin ordering in stripes is well established by neutron diffraction for La$_{2-x}$Sr$_x$NiO$_4$ at several charge doping levels x between 0.135 and 0.55 [31–33]. In μSR studies by Chow *et al* [35] and Jestaedt *et al* [38] the doping dependence of the magnetic ordering temperature has been measured over a wide doping range ($0 \leqslant x \leqslant 1$). The time
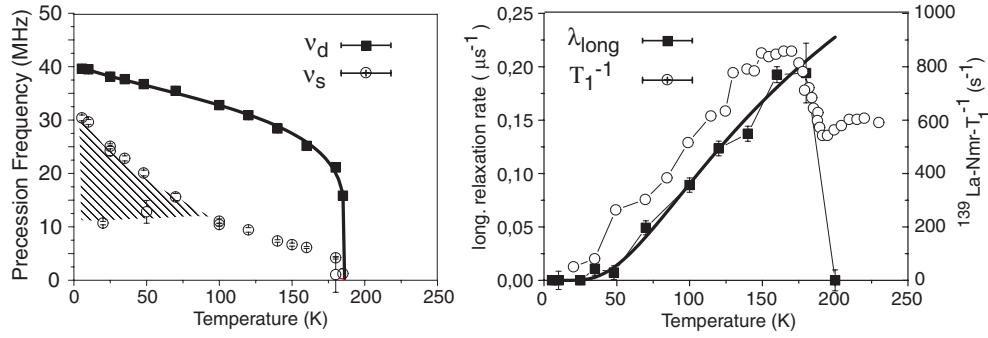
Figure 5. Temperature dependence of the spontaneous muon spin precession frequencies ν_d and ν_s (left panel) in $La_{1.66}Sr_{0.33}NiO_4$. The solid curve represents a fit with a critical behaviour, resulting in $T_{mag} = 187.5(10)$ K and $\nu_d(0) = 40.8(8)$ MHz. The shaded area indicates the broadening of the stripe signal below 100 K. The right-hand panel shows the longitudinal relaxation rate λ_{long}. The solid curve represents a fit with $\lambda_{long} \propto \exp(-E_a/T)$ and $E_a = 185$ (20) K, and the open circles indicate the ^{139}La-NMR-T_1 relaxation rate measured on the same crystal by Yoshinari *et al* [42].

spectra in the ordered state have been analysed with a single strongly relaxing muon precession signal to derive the temperature dependence of the sublattice magnetization and the mean spin fluctuation rate. In consecutive experiments on a single crystal with $x = 0.33$ and several polycrystalline specimens with $0.2 \leqslant x \leqslant 0.6$, we focused on an analysis of the shape and structure of the muon precession frequency distribution to identify a signature of the inhomogeneous stripe order [39].

The single crystal with $x = 0.33$ showed spontaneous muon spin precession below 190 K with a very strong static relaxation. Between 70 and 185 K we identified two distinct signals with low temperature saturation values of the spontaneous muon precession frequencies of $\approx$40 MHz and $\approx$15 MHz. The time spectra were analysed using a muon spin-polarization function of the form

$$A(t) = A_{rot,d} \cos(2\pi\nu_d t) \exp(-\lambda_{t,d}t) + A_{rot,s} \cos(2\pi\nu_s t) \exp(-\lambda_{t,s}t) + A_{long} \exp(-\lambda_{long}t)$$
(1)

where $A_{rot,(d,s)}$, $\nu_{(d,s)}$ and $\lambda_{t,(d,s)}$ represent the amplitude, frequency and transverse relaxation rate of signals associated with muons having a nearest neighbour Ni^{2+} or Ni^{3+} ion. In the spin stripe picture these sites are located in the AF domains (d) and non-magnetic charge stripes (s), respectively. This interpretation of the two precession signals is supported by the relative intensities of 0.65 and 0.35 for the domain and charge stripe signals, which correspond perfectly to the expectation of 0.33 for the hole doped Ni^{3+} site. A_{long} and λ_{long} describe the non-precessing signal amplitude and the longitudinal relaxation rate due to muons experiencing a local magnetic field parallel to their initial spin-polarization.

Figure 5 shows the temperature dependence of $\nu_{(d,s)}$ and λ_{long}. Above 70 K we find a finite muon precession frequency of the non-magnetic domain wall signal of $\nu_s \approx 1/3\nu_d$. In an idealized stripe ordered state (see figure 1) and assuming a relevant muon hyperfine coupling to the nearest Ni spin only a signal at zero frequency would be expected for muons bound to an apical oxygen directly above or below an Ni ion in a domain wall. The finite value of ν_s can be explained by a finite value of the spin-polarization of the $S = 1/2$ Ni^{3+} hole states in the domain walls and additional finite hyperfine coupling of the muon to the next nearest neighbour Ni^{2+} spins.

The frequency spectra exhibit a characteristic change below 100 K (see figure 4) where the domain wall signal broadens considerably. Polarized neutron scattering experiments by Lee *et al* [52] have revealed a considerable canting of the Ni^{2+} spins away from the [110] direction of the charge stripes. At 80 K a step in the spin canting and an increase of the charge and spin superlattice peaks is observed. This is interpreted as a lock-in of the charge superstructure into a fully commensurate modulation.

To study the hole doping dependence we examined a series of polycrystalline powder samples with $0.2 \leqslant x \leqslant 0.6$. The magnetic ordering temperatures T_{mag} of these samples are in good agreement with those reported by Jestaedt *et al* in [38]. In particular, T_{mag} exhibits a sharp maximum at $x = 0.33$. Also the muon spin precession frequency ν_d ($T \rightarrow 0$) in the magnetic domain shows a 15% enhanced value at $x = 0.33$. Both observations document the specific stability of the commensurate stripe order at $x = 0.33$. At 50 K the frequency spectra reveal a well-defined low frequency peak only for $0.25 \leqslant x \leqslant 0.40$ [39]. This indicates that a spin structure with fully localized antiphase domain walls is restricted to this concentration range.

3.3. Spin dynamics in $La_{1.67}Sr_{0.33}NiO_4$

The longitudinal relaxation rate λ_{long} reveals a strong decrease with decreasing temperature in the magnetically ordered phase below 190 K. For a homogeneous spin system without additional (charge) degrees of freedom, a peak at the ordering temperature and a weak longitudinal relaxation in the ordered state are expected. This is interpreted as a coupling of the muon spin to spin waves in the fast fluctuation limit. In this picture a reduction of λ_{long} with decreasing temperature is associated with a reduction of the amplitude of the field fluctuation at the muon site, i.e., the thermal occupation of magnons. However, in doped transition metal oxides the motion of the charge carriers can give rise to an independent dynamic relaxation contribution. In particular, this is the case if the system is antiferromagnetically ordered. Then, each hopping process of the doped charges is accompanied by a spin hopping in the opposite direction. The local field at nearby muon sites can change drastically in amplitude and orientation. To explain the behaviour in $La_{1.67}Sr_{0.33}NiO_4$ we consider such an additional fluctuating magnetic field at the muon site caused by charge hopping processes. In good approximation this can be described by an isotropic static line width σ_{stat} and a temperature dependent fluctuation rate ν_C. σ_{stat} is interpreted as an effective line width at the muon site which is strongly charge carrier concentration dependent but more or less independent of the temperature. The fluctuation rate is a measure of the local charge fluctuation and can be strongly temperature dependent, e.g. due to activated charge hopping processes. For fast fluctuations ($\sigma_{stat} \ll \nu_C$) the longitudinal relaxation λ_{long} can be calculated using Redfield theory [43–45]. In the framework of this theory a maximum of λ_{long} is expected for $\nu_C = \omega_\mu$. As we will see in section 4.2 below (figure 12), this maximum is observed in magnetically ordered $La_{2-x}Sr_xCuO_4$ and $La_{2-x-y}Eu_ySr_xCuO_4$ cuprates where the charge mobility is much higher. Since in $La_{1.67}Sr_{0.33}NiO_4$ λ_{long} monotonically increases with increasing temperature throughout the magnetically ordered phase, and also ν_C is expected to rise with increasing temperature, we assume that we are in a slow fluctuation regime $\nu_C < \omega_\mu$. In this regime Redfield theory states that λ_{long} is proportional to ν_C. The temperature dependence of λ_{long} can be described by a thermally activated process $\lambda_{long} \propto \exp(-E_a/T)$ with $E_a = 185$ (20) K. A similar behaviour is found for the ^{139}La-NMR-T_1 relaxation rate [42] in the same crystal. We associate this behaviour with the freezing of transverse fluctuations of the charge stripes in the charge ordered state. Such a stripe liquid has also been deduced from neutron scattering experiments on $La_{2-x}Sr_xNiO_4$ with $x = 0.275$ [46].
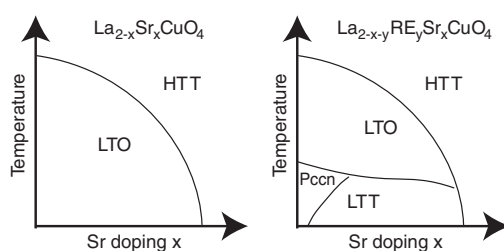
Figure 6. Structural phase diagrams of $La_{2-x}Sr_xCuO_4$ and $La_{2-x-y}RE_ySr_xCuO_4$.

4. Spin stripe correlations in rare-earth doped $La_{2-x}Sr_xCuO_4$

Small structural differences have a drastic influence on the electronic ground state in the $La_{2-x}Sr_xCuO_4$ cuprates. Therefore we first summarize some basic facts about the structural modifications in $La_{2-x}Sr_xCuO_4$ (see e.g. [47]). The tetragonal K_2NiF_4 structure is found in La_2CuO_4 only above $T_{LT} \approx 500$ K. It is denominated as the high temperature tetragonal (HTT) phase. Below T_{LT} the CuO_6 octahedra are tilted along a [110] axis in the CuO_2 planes. This phase with an orthorhombic distortion is called the low temperature orthorhombic (LTO) phase. The transition is associated with a mismatch of the Cu–O(1) and La–O(2) bond lengths in the ab-planes. This mismatch and subsequently the octahedral tilt angle Φ are reduced by partially substituting the La^{3+} with the larger Sr^{2+} ion. Consequently also T_{LT} decreases with increasing Sr content (see figure 6).

A partial substitution of La^{3+} in $La_{2-x}Sr_xCuO_4$ with the smaller rare-earth ions Nd^{3+} or Eu^{3+} increases the bond length mismatch. At low temperatures this leads to a change of the CuO_6 tilting geometry. The orientation of the tilting axis changes from [110] in every plane to an alternation of [100] and [010] in every second plane. Therefore a global tetragonal symmetry is recovered and this phase is called the low temperature tetragonal (LTT) phase. For small Sr doping yet a phase with not fully equivalent a and b axes is found which is called $Pccn$ or LTLO (low temperature less orthorhombic) phase.

Now we turn to the electronic properties. In the LTT phase superconductivity (SC) is suppressed [54] and static AF occurs in compounds with large hole content. This is observed in a small doping range around $x = 1/8$ in the series $La_{2-x}Ba_xCuO_4$ [48–50, 14] where the LTT phase is found in a fraction of the sample volume between $x = 0.10$ and 0.20. We performed a systematic examination of the electronic properties of the LTT phase in a much wider doping range which is possible in the rare-earth doped $La_{2-x}Sr_xCuO_4$. In this class of compounds static spin and charge stripes are inferred from neutron and x-ray diffraction investigations of the LTT phase [1, 2].

It has been argued that the LTT structure provides a pinning potential for the stripe motion, and the changes of the electronic properties at the LTO to LTT phase transition are attributed to a change from dynamic to static stripes [1, 5]. In this section we present experimental evidence that in $La_{2-x-y}Nd_ySr_xCuO_4$ and $La_{2-x-y}Eu_ySr_xCuO_4$ the CuO_6-octahedra tilt angle Φ in the LTT phase is the relevant parameter which controls the pinning potential. Below a critical value Φ_C bulk superconductivity is found, and above Φ_C static magnetic stripe order suppresses superconductivity.

4.1. μSR spectra of spin stripe ordered cuprates

Static spin stripe order in cuprates has been discovered by neutron scattering experiments on $La_{2-x-y}Nd_ySr_xCuO_4$. The doped Nd^{3+} ions are paramagnetic ($J = 9/2$, Kramers ground
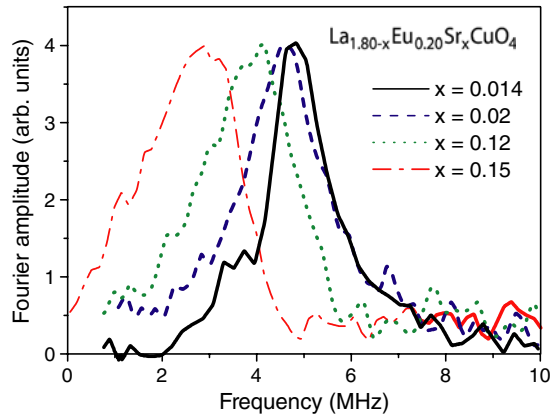
Figure 7. Zero field μSR frequency spectra at $T = 2$ K for $La_{1.8-x}Eu_{0.2}Sr_xCuO_4$ with $x = 0.014$, 0.02, 0.12 and 0.15.

state with $\mu_{eff} \approx 1.3\ \mu_B$). These fluctuating magnetic moments give rise to an additional relaxation of the muon spin superimposed on the relaxation caused by the Cu magnetism. In contrast, Eu^{3+} has a $J = 0$ ground state with a very weak Van Vleck paramagnetic moment which does not contribute significantly to the static and dynamic local fields at the muon site. Therefore, the μSR signal is determined by the hyperfine interaction with the Cu spin system alone and $La_{2-x-y}Eu_ySr_xCuO_4$ is much better suited to examine a characteristic signature of spin stripe order.

In figure 7 we show representative zero field μSR frequency spectra of $La_{1.8-x}Eu_{0.2}Sr_xCuO_4$ for Sr concentrations $x = 0.014$ (long-range AF phase), 0.02 (short-range AF phase) and $x = 0.12$, 0.15 (AF spin stripe phase). For $x = 0.014$ a symmetric spectrum of Lorentzian shape centred at 4.9 MHz is found, as is observed in $La_{2-x}Sr_xCuO_4$ [24]. The frequency spectrum in the short-range ordered phase exhibits a maximum at the same frequency with an asymmetrically increased low frequency tail.

In the spin stripe ordered regime the ZF frequency spectra do not show well separated signals for the magnetic domains and charge stripes as observed in the stripe ordered nickelate $La_{1.67}Sr_{0.33}NiO_4$. The spectra are similar to those in the short-range ordered phase. The maximum is shifted to lower frequencies and the asymmetric broadening is more pronounced. This demonstrates the similarity of these phases: a nanoscale coexistence of non-magnetic and magnetic Cu sites. The similarity also holds on a larger scale since recent neutron scattering experiments have revealed 1D stripe correlations of charge and spin also in the short-range ordered phase of $La_{2-x}Sr_xCuO_4$ [63].

We have performed simulations of the local field distribution for a commensurate spin stripe ordered system with $x = 1/8$ with site or bond centred charge stripes at different muon sites, taking into account dipole fields from static Cu moments within a sphere of 60 Å radius. The Cu spins with a magnitude of 0.5 μ_B and sinusoidal modulation were aligned along the [110] direction. Typical results are depicted in figure 8. For a muon site (0.253, 0.0, 0.162) deduced for $La_{2-x}Sr_xCuO_4$ [59] and using a Lorentzian broadening of 1 μs^{-1} a distinct multiple line spectrum is found, in good agreement with [59]. These simulated spectra change dramatically if a slightly different site is used. Assuming a site (0.225, 0.0, 0.225), slightly further away from the nearest Cu site, we find a continuous asymmetrically broadened frequency distribution of similar shape, as observed experimentally. However, the maximum is 2 MHz below the measured value, since in this case the distance to the nearest neighbour
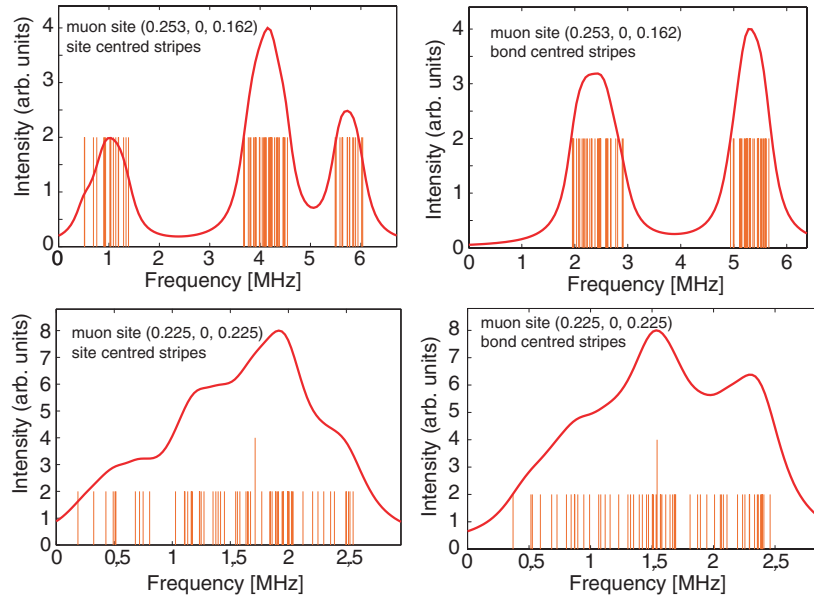
Figure 8. Calculated muon frequency distributions for a commensurate spin stripe ordered system with a spin periodicity of eight lattice constants, site or bond centred charge stripes and sinusoidal modulation of the ordered moment magnitude for two possible muon sites.

Cu site is too large. These results show how sensitively the frequency distribution depends on the assumed muon site. In $La_{2-x-y}Eu_ySr_xCuO_4$ a site intermediate between the two sites analysed here is very likely.

4.2. Electronic phase diagrams

Following the neutron scattering studies by Tranquada *et al* [1], several μSR experiments on $La_{2-x-y}Nd_ySr_xCuO_4$ have been reported. Wagener *et al* [55, 56] confirmed a magnetic ground state for $x = 0.15$ and $y \geqslant 0.30$, Luke *et al* [57] and Lappas *et al* [58] compared the magnetic order for $x = 0.125$ with and without Nd doping. Nachumi *et al* [59] compared different charge carrier dopings $x \geqslant 0.125$ at $y = 0.4$ and found a coexistence of spin stripe order and superconductivity at $x = 0.20$ within this series. We focused on a search for static AF order in a wide range of Nd doping y and Sr doping x using polycrystalline samples. The aim was to determine relevant structural and electronic parameters for the stability of spin stripe order.

Figure 9 shows typical ZF time spectra measured for $y = 0.6$ and $x = 0.15$. The spectra were analysed using a phenomenological polarization function with two cosine precession frequencies, i.e.,

$$A(t) = A_0[\tfrac{2}{3}f_{mag}\{f_1\cos(2\pi\nu_1 t)\exp(-\lambda_{t,1}t) + f_2\cos(2\pi\nu_2 t)\exp(-\lambda_{t,2}t)\}$$
$$+ (1 - \tfrac{2}{3}f_{mag})\exp(-\lambda_{long}t)]. \tag{2}$$

In this analysis ν_1 represents the maximum of the internal field distribution, which gives an appropriate measure for the magnetic field at the muon site and thus allows the staggered magnetization of the Cu spins to be determined. ν_2 is $\approx 1/2\,\nu_1$ and describes the asymmetrically increased low frequency tail. Below 10 K the Nd spins develop a static component due to the molecular field caused by the Cu spin system. Since the Nd is randomly distributed in the lattice it results in an increase of the static and dynamic relaxation rate. It also causes a
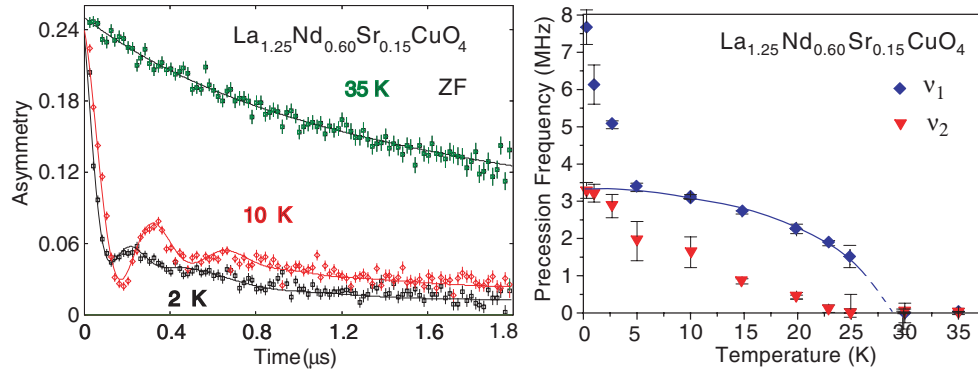
Figure 9. Typical ZF-μSR time spectra for stripe ordered La$_{2-x-y}$Nd$_y$Sr$_x$CuO$_4$ at different temperatures (left-hand panel). The solid curves represent fits as described in the text. The right-hand panel depicts the temperature dependence of the deduced precession frequencies.

strong increase (factor 2 and more) of the muon precession frequency below 10 K as observed in electron doped Nd$_2$CuO$_4$ [44]. In addition the Cu spin-canting out of the (001) plane as suggested by neutron scattering on the spin stripe ordered compounds [62] can contribute to the increase of the muon precession frequency below 10 K.

Neutron scattering experiments on La$_{2-x-y}$Nd$_y$Sr$_x$CuO$_4$ reveal a spin stripe superstructure which (except for $x = 0.125$) is incommensurate with the crystal lattice [62]. In this case the resulting local magnetic field distribution at the muon site is continuous, with one pronounced maximum at the highest field. In the time domain this leads to a zeroth order Bessel instead of the cosine relaxation function. Such a fit function results in a poor description of our data. Nachumi *et al* [59] and Lappas *et al* [70] have used Bessel and single frequency cosine functions successfully to describe experiments on La$_{2-x-y}$Nd$_y$Sr$_x$CuO$_4$ with $y = 0.4$ and $x = 0.125, 0.15$ and on La$_{1.875}$Ba$_{0.125-y}$Sr$_y$CuO$_4$.

Figure 10 shows the phase diagram of La$_{2-x-y}$Nd$_y$Sr$_x$CuO$_4$ at optimum charge carrier doping $x = 0.15$ as a function of the Nd doping, y. For low y a superconducting LTO phase is found with a small decrease of T_C with increasing Nd content. Above the structural phase boundary at $y \approx 0.16$ all samples show a 100% magnetically ordered volume below 10 K. The magnetic ordering temperature as well as the muon spin precession frequency at 10 K are nearly independent of y. This figure proves the strong correlation of the crystal structure with the electronic ground state in the La$_{2-x}$Sr$_x$CuO$_4$ system. A closer look at this transition from superconducting to magnetic ground state as a function of the value of the LTT tilt angle is presented in section 4.3 below for the La$_{2-x-y}$Eu$_y$Sr$_x$CuO$_4$ system.

Studies on a second series of samples with a fixed Nd content $y = 0.6$ as a function of the charge carrier doping $0.12 \leqslant x \leqslant 0.20$ reveal a suppression of the muon precession frequency for increasing charge doping, x. Note that increasing the Sr content x not only increases the number of charge carriers but also reduces the CuO$_6$ octahedra tilt angle. Therefore in doping studies of this kind a clear separation between structural and electronic doping effects on the ground state is not possible. For $x = 0.20$ no coherent muon spin precession is observed. Yet a strong transverse relaxation of 2/3 of the sample signal with $\lambda_T \approx 30\ \mu$s^{-1} and weak longitudinal relaxation $\lambda_{\text{long}} = 1.0(1)\ \mu$s^{-1} at 10 K indicates a strongly disordered but quasi-static Cu spin system. All samples studied show a 100% magnetic volume fraction at 10 K, resulting in the phase diagram presented in figure 11.

Nachumi *et al* [59] studied single crystals of La$_{2-x-y}$Nd$_y$Sr$_x$CuO$_4$ *with a smaller Nd content $y = 0.4$ and $x = 0.125, 0.15$ and 0.20 by μSR. The ZF-μSR spectra of the samples*

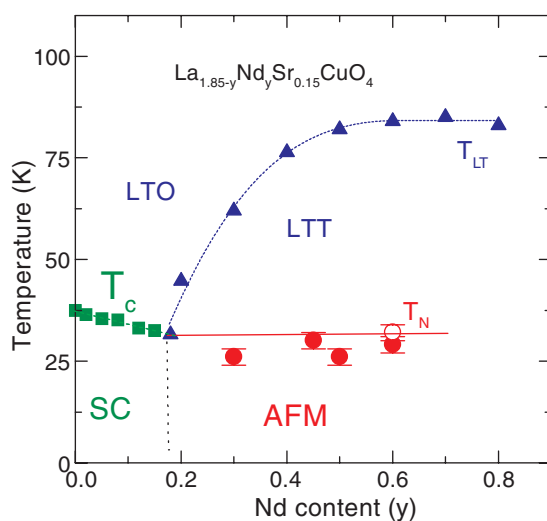**Figure 10.** The phase diagram of $La_{2-x-y}Nd_ySr_xCuO_4$ with $x = 0.15$. Triangles indicate the structural transition from LTO to LTT, squares denote the superconducting T_C from magnetization experiments, and closed circles the magnetic transition temperatures derived from μSR [55].
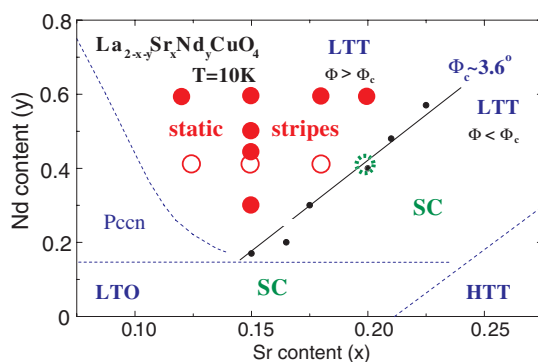

Figure 11. Structural and electronic phase in $La_{2-x-y}Nd_ySr_xCuO_4$ at 10 K as function of Nd doping, y, and Sr doping, x. The full circles indicate the compositions studied by μSR in this work. The open circles indicate compositions studied by Nachumi *et al* [59]. The green dashed open circle indicates that this composition is non-magnetic at 10 K. It shows quasi-static muon spin relaxation below 2 K only. The full diagonal line indicates a constant octahedra tilt angle $\Phi_C = 3.6°$ in the LTT phase. Bulk superconductivity is found in the LTT phase only for $\Phi < \Phi_C$ [54].

with $x = 0.125$ and 0.15 are very similar to the spectra in figure 9. The deduced muon spin precession frequencies at 10 K are $\approx$0.5 MHz larger than in our studies, since a Bessel function was used for the data analysis. For $y = 0.4$ and $x = 0.20$, only at $T = 1.9$ K was a quasi-static behaviour observed, similar to our results for $y = 0.6$, $x = 0.20$ at 10 K. This difference is fully consistent with the critical tilt angle picture and the phase diagram presented in figure 11. The smaller Nd content causes an already reduced LTT tilt angle. Therefore the critical LTT tilt angle is reached at a lower Sr content and the composition $y = 0.4$, $x = 0.20$ is located right at the critical tilt angle line in figure 11.

On $La_{2-x-y}Eu_ySr_xCuO_4$ with $y = 0.20$ we performed a systematic μSR study in a wide charge carrier doping range ($0 \leqslant x \leqslant 0.2$) [51, 68]. For all samples x-ray diffraction data show
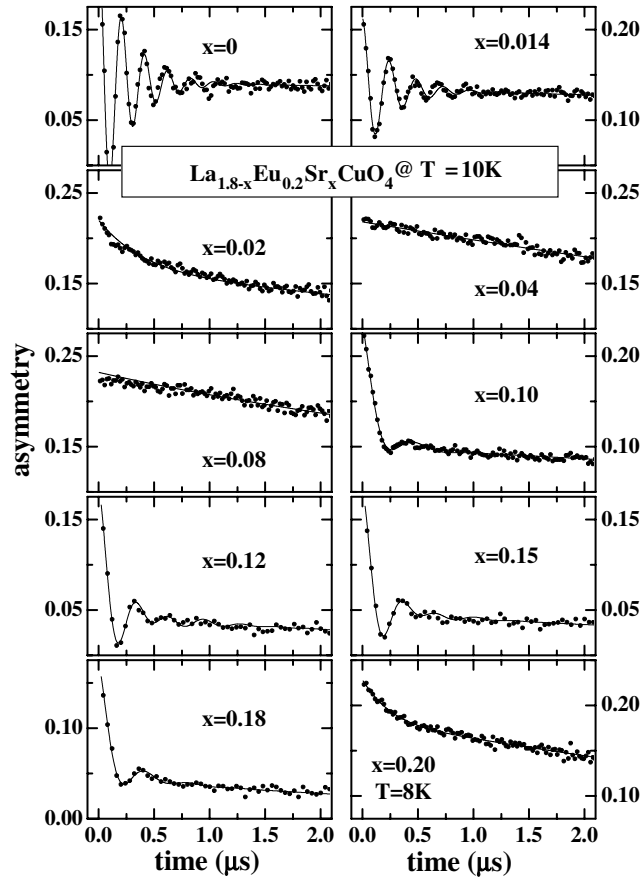
Figure 12. Zero field μSR spectra at 10 K for $La_{2-x-y}Eu_ySr_xCuO_4$ with $0 \leqslant x \leqslant 0.20$. The solid curves are fits as described in the text [51].

an LTT structure at low temperature with an LTO $\rightarrow$ LTT transition temperature $T_{LT} \simeq 125$ K nearly independent of x. No superconductivity is found for $x < 0.15$, whereas for higher doping traces of SC are observed in resistivity and susceptibility measurements [20]. Typical ZF-μSR time spectra at 10 K are displayed in figure 12.

At zero and small Sr doping $0 \leqslant x \leqslant 0.02$ the μSR experiments reveal no significant differences for the transition temperatures to the long-range AF state in comparison with $La_{2-x}Sr_xCuO_4$. For all samples the low temperature spectra are analysed without a non-magnetic signal fraction. A single muon precession frequency signal with exponential relaxation is used. For $0.014 \leqslant x \leqslant 0.018$, specific low temperature anomalies are observed deep in the AF ordered state similar to the $La_{2-x}Sr_xCuO_4$ system [24]: an upturn of the muon precession frequency ν below 25 K which is accompanied by a maximum in λ_{long} at ≈ 7 K (figure 13). μSR experiments on Zn doped $La_{2-x}Sr_xCuO_4$ prove that both anomalies are connected to the localization of combined spin/charge fluctuations in the CuO_2 planes [53, 69] similar to those proposed by Borsa *et al* [24]. Recent neutron scattering studies revealed the formation of static spin stripes in the AF long-range ordered phase below 50 K [64]. It implies the existence of static charge stripes at low temperatures. In this picture the reduced muon precession frequency above 30 K is a consequence of fluctuating charge stripes which itself
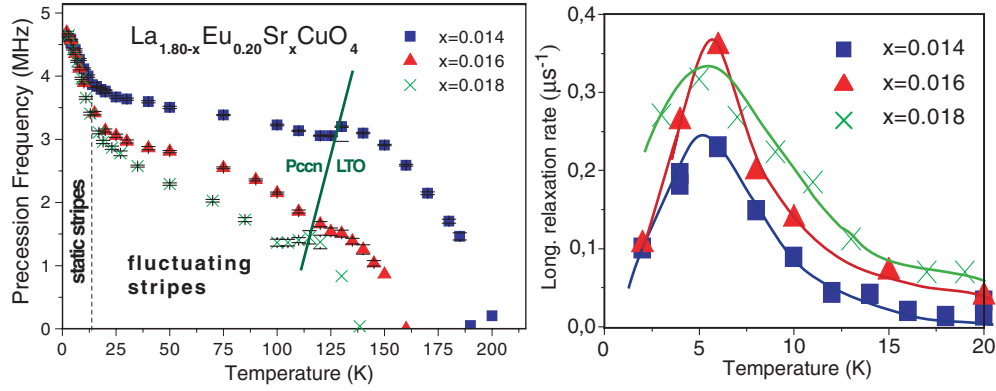
Figure 13. Temperature dependences of the muon precession frequency ν_1 (left-hand panel) and the longitudinal relaxation rate λ_{long} (right-hand panel) in $La_{1.8-x}Eu_{0.2}Sr_xCuO_4$ with $x = 0.014$, 0.016 and 0.018. The curves are guides to the eyes only.
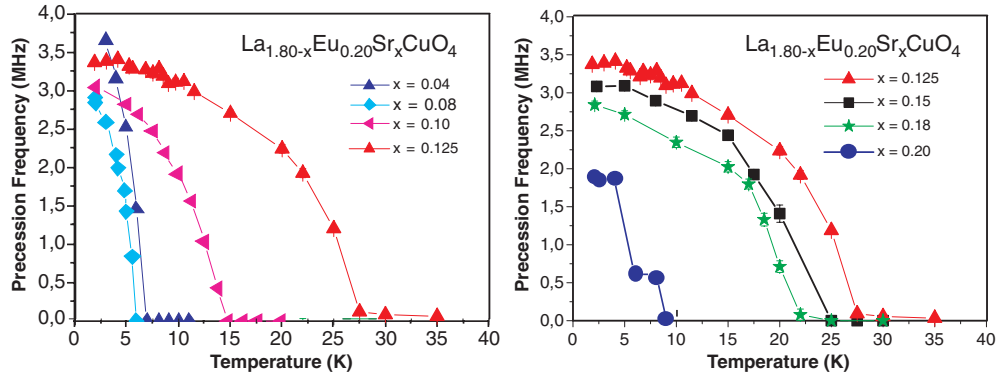

Figure 14. Temperature dependence of the muon precession frequency ν_1 in $La_{1.8-x}Eu_{0.2}Sr_xCuO_4$ with $0.04 \leqslant x \leqslant 0.20$. The lines represent guides to the eyes only.

may exist up to much higher temperatures. In contrast to the nickelate $La_{1.67}Sr_{0.33}NiO_4$ we do observe a pronounced maximum of the dynamic relaxation rate (right-hand panel of figure 13) deep in the magnetically ordered phase (T_N is between 130 and 200 K for these samples), which proves that an independent magnetic fluctuation process with a strongly temperature dependent fluctuation rate is present. At 7 K this fluctuation rate is equal to $2\pi\nu_\mu \approx 25$ MHz. We associate this very low fluctuation rate with collective transversal fluctuations of the charge stripes, i.e., the antiphase domain walls in the AF ordered system. A quantitative analysis is presented in section 4.4.

The analysis of the μSR time spectra for $x \geqslant 0.02$ is done using the two-frequency signal described above (equation (2)). In the concentration range $0.02 \leqslant x \leqslant 0.05$ with short-range static magnetic order also no significant differences between the LTT and the LTO phases are found. Drastic differences show up upon further increasing the doping. Whereas the ordering temperature as determined from μSR data decreases monotonically in $La_{2-x}Sr_xCuO_4$ [25, 61], we find an increase of T_N with increasing hole content in $La_{2-x-y}Eu_ySr_xCuO_4$. For samples with $0.04 \leqslant x < 0.20$ the muon spin precession frequency ν_1 follows a typical temperature dependence of an order parameter and does not show any

anomalies at low T (see figure 14). In particular, there is no further increase of ν_1 at $T \ll T_N$ as observed for $x \leqslant 0.02$. The absolute values of ν_1 for $T \to 0$ are very similar in the concentration range $0.08 \leqslant x < 0.18$ and indicate a nearly concentration independent $T = 0$ sublattice magnetization in this range of doping. Though T_N is one order of magnitude smaller than for undoped (La, Eu)$_2$CuO$_4$, and though there are many mobile holes [60], the values of ν_{sat} amount to about 70% of the frequency found in the Néel state for $x = 0$. This is qualitatively consistent with the calculations of the magnetic properties of CuO$_2$ planes with a static stripe order in [65].

The phase diagrams of pure and Eu doped La$_{2-x}$Sr$_x$CuO$_4$ reveal a striking similarity. In a wide doping range the superconducting phase of La$_{2-x}$Sr$_x$CuO$_4$ seems to be replaced by the stripe AF in La$_{1.8-x}$Eu$_{0.2}$Sr$_x$CuO$_4$. In the LTO phase superconductivity occurs for $x > 0.05$ and T_c increases with increasing hole content. In the same range of hole doping we observe an increase of the static magnetic order in the LTT phase and even the ordering temperatures T_N compare well with T_c found in the LTO phase, i.e., $T_N^{LTT}(x) \sim T_c^{LTO}(x)$. Thus, by changing the structure from LTO to LTT it is possible to switch from SC to AF with a nearly unchanged critical temperature. For $x = 0.15$ this switching with the same critical temperature has also been observed in Nd doped La$_{2-x}$Sr$_x$CuO$_4$ as described above.

The phase diagram (figure 15) shows that the change from SC to AF does not only occur due to the LTO → LTT transition, but also within the LTT phase if the hole doping is slightly increased from $x = 0.18$ to 0.2. T_N drops substantially and a reduced $\nu_{1,sat} \simeq 1.7$ MHz is found (see figure 15). In the same range of doping there is also a pronounced change of SC. For $x = 0.2$ susceptibility measurements exhibit enhanced shielding signals [20]. This transition will be examined more closely in the following section.

4.3. The interplay of spin stripe order and superconductivity

In this section we present further evidence for the correlation of the electronic ground state in La$_{2-x-y}$Eu$_y$Sr$_x$CuO$_4$ with the octahedra tilt angle Φ *within* the LTT phase. To discriminate the influence of hole doping [66] and tilt distortion [54] we have studied the series La$_{1.80-y}$Eu$_y$Sr$_{0.20}$CuO$_4$, i.e., samples at fixed carrier concentration $x = 0.20$ with a variable Eu content $0.10 \leqslant y \leqslant 0.23$, thereby increasing only the LTT tilt angle [68]. Figure 16 shows typical ZF spectra for $y = 0.10$ and 0.23 at different temperatures. At $y = 0.10$ only a weak magnetic muon spin relaxation is observed in $\approx$50% of the sample volume at 2 K, whereas at $y = 0.23$ a strong static magnetic relaxation of the full sample signal is found below 5 K. The evaluated magnetic volume fractions are depicted in figure 17. Clearly the magnetic ordering temperature is increasing with increasing Eu doping, i.e., for larger octahedra tilt angles. The width of the static local field distribution at the muon site also increases with stronger Eu doping. Only for $y = 0.23$ is an asymmetrically broadened frequency spectrum with a maximum at a finite frequency observed at 2 K. For $y = 0.20$ and 0.23 a nonzero spontaneous muon spin precession can be extracted from the data, which is impossible for smaller Eu content, i.e., smaller tilt distortion [68].

Since in La$_{2-x-y}$Eu$_y$Sr$_x$CuO$_4$ a dynamic relaxation of the muon spin-polarization due to a rare-earth magnetic moment is absent, it is possible to study the magnetic penetration depth λ of the type-II superconductors in the vortex state above H_{c1} via TF-μSR [26]. In a qualitative approach for polycrystalline specimens of extreme type-II superconductors ($\lambda \gg \xi$, where ξ is the coherence length of the superconductor) the muon spin-polarization is proportional to $\exp(-\sigma^2 t^2)$, and for the measured static Gaussian relaxation rate one finds $\sigma \propto 1/\lambda^2 \propto n_s$ [26]. Therefore, in the absence of magnetic relaxation σ can be used as a measure of the density of superconducting carriers n_s.
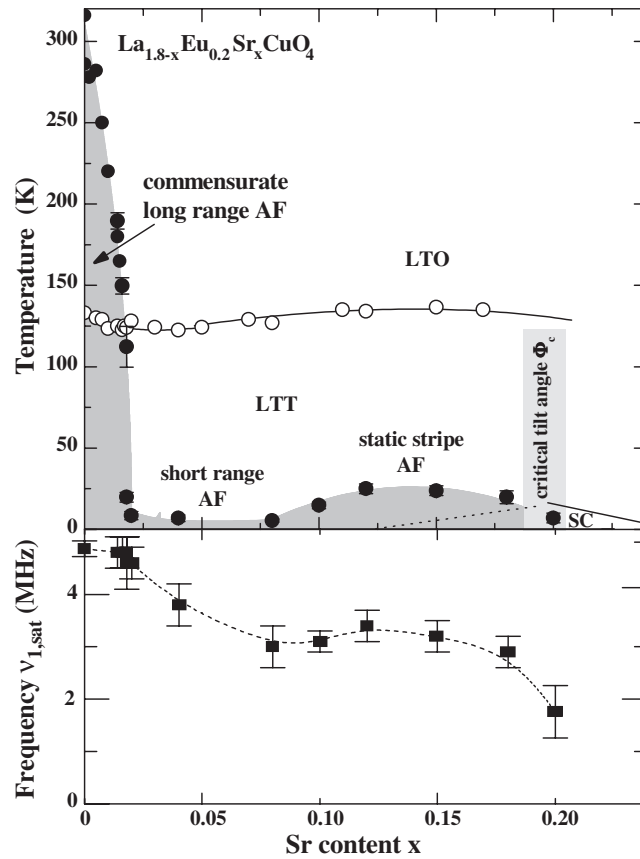
Figure 15. Phase diagram of $La_{1.8-x}Eu_{0.2}Sr_xCuO_4$ and saturation frequency ν_{sat} as a function of x. Full and open circles denote the magnetic and the structural (LTO $\rightarrow$ LTT) transition temperatures, respectively. In the upper viewgraph the solid (dotted) curve marks the region with strong (weak) diamagnetic signals due to superconductivity [20].
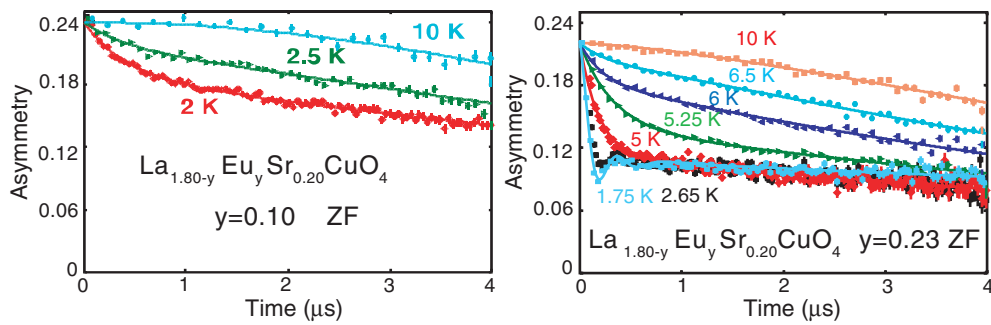

Figure 16. ZF spectra of $La_{1.80-y}Eu_ySr_{0.20}CuO_4$ with $y = 0.10$ and 0.23 at different temperatures.

We performed TF-μSR in 2000 G external magnetic field on all samples of this series. The results for σ are shown in the right-hand panel of figure 17. σ strongly increases close to the magnetic transition temperature T_{mag} due to critical magnetic fluctuations. Above T_{mag} and
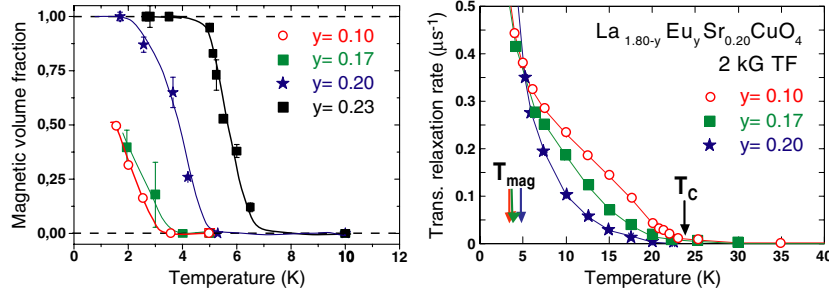
Figure 17. Magnetic signal fraction extracted from the ZF spectra La$_{1.80-y}$Eu$_y$Sr$_{0.20}$CuO$_4$ (left-hand panel) and temperature dependence of the muon relaxation rate in 2 kG TF experiments.

below $\approx$22 K a different behaviour is observed. On reducing the Eu content to $y = 0.17$ and 0.10, σ is enhanced and shows a negative curvature. Since the magnetic order is suppressed by lowering y, this increase of σ is due to an increase of the *average* n_s in the sample.

Due to the small absolute values of σ it was not possible to differentiate non-superconducting and superconducting signal fractions. Therefore the increase of σ can either be due to an increase of n_s in a constant volume fraction of the sample or to an increase of the superconducting volume fraction for constant n_s. In combination with the measured magnetic volume fractions the latter interpretation is more reasonable, and an Eu doping dependent phase separation in superconducting and magnetic volume fractions is deduced.

This result is further supported by μSR experiments by Kojima *et al* [71]. The authors studied a series of La$_{2-x-y}$Eu$_y$Sr$_x$CuO$_4$ at a fixed charge carrier content $x = 0.15$ for various y. In full agreement with our results, a reduction of n_s and an increase of the magnetic volume fraction at low temperatures was found for increasing y.

These data prove unambiguously that increasing the LTT tilt angle of the CuO$_6$ octahedra causes a change from a superconducting to a magnetic ground state. We conclude that the change from a state with dynamic spin fluctuations to one with static stripe order in the system La$_{1.8-x}$Eu$_{0.2}$Sr$_x$CuO$_4$ is not only observed at a specific charge carrier concentration x as assumed for example in [66].

Furthermore, the phase coexistence of superconductivity and magnetic stripe order at finite temperatures does not support a quantum critical point of the AF ordered phase as observed for example in some heavy fermions. It could be described by a first order phase transition with a tri- or tetracritical point, depending on the source of the phase coexistence: spatial inhomogeneity of the control parameter Φ or intrinsic electronic phase separation [67].

4.4. Slow fluctuations of a stripe liquid

In La$_{2-x-y}$Eu$_y$Sr$_x$CuO$_4$ it is possible to deduce the dynamics of the Cu spin system from a detailed analysis of the longitudinal relaxation rate λ_{long}. For most samples in the doping range $0.02 \leqslant x \leqslant 0.18$ the longitudinal relaxation rate λ_{long} exhibits a broad maximum at the magnetic ordering temperature with a slow monotonic decrease towards $T = 2$ K. Only for $x = 0.15$ is an isolated second maximum at $\approx$12 K observed in the spin stripe ordered phase (see figure 18) which resembles the low temperature anomaly found in the long-range AF phase at $x < 0.02$ (see figure 13).

These peaks in λ_{long} can be analysed assuming a slowing down of Cu spin fluctuations with a static line width σ_{stat} and a mean fluctuation rate ν_C in a Redfield analysis [43]. In the
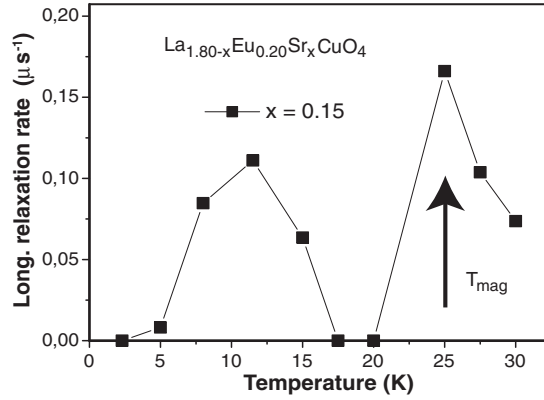
Figure 18. Temperature dependence of the longitudinal relaxation rate λ_{long} in $La_{1.8-x}Eu_{0.2}Sr_xCuO_4$ with $x = 0.15$. The curve represents a guide to the eyes only.
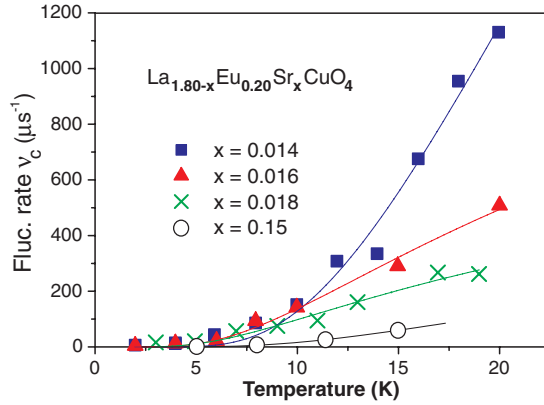

Figure 19. Temperature dependence of the local field fluctuation rate ν_C calculated with equation (3). The curves are fits using a thermally activated behaviour.

magnetically ordered state the Cu spins and the muon spin precess in their local exchange field $\omega_{\text{Cu}} = \gamma_e B_{\text{Cu}}$ and dipole field $\omega_\mu = \gamma_\mu B_{\text{loc}}$, respectively. Since $\omega_{\text{Cu}} \gg \omega_\mu$ the longitudinal relaxation rate is given by [44]

$$\lambda_{\text{long}} = \frac{3}{2}\sigma_{\text{stat}}^2 \frac{\nu_C}{\nu_C^2 + \omega_\mu^2}. \tag{3}$$

Since $\omega_\mu = 2\pi\nu_1$ is known from the analysis of the μSR time spectra the static width σ_{stat} can be calculated from the maximum for λ_{long} in equation (3), where $\nu_C = \omega_\mu$ holds. Consecutively the temperature dependence of ν_C can be evaluated. The results for $x = 0.014, 0.016, 0.018$ and 0.15 are presented in figure 19, and are well described by a thermally activated behaviour of the form $\nu_C = \nu_\infty \exp(E_a/k_B T)$. The results of these fits are compared with those obtained for $La_{1.67}Sr_{0.33}NiO_4$ in table 1.

The low temperature spin fluctuations are found only in the charge carrier doped systems. We associate them with the dynamic fluctuations causing the wipeout in Cu-NMR [18] or the glassy dynamics observed in La-NMR [16] and Gd-EPR [20]. Since in particular for the low doped samples it seems rather unlikely that individual hole motion can cause such drastic effects in the time window of the μSR method, we associate the collective transverse

Table 1. Parameters describing the thermally activated spin fluctuations in $La_{1.67}Sr_{0.33}NiO_4$ and $La_{1.8-x}Eu_{0.2}Sr_xCuO_4$.

Sample	Doping x	σ_{stat} (μs^{-1})	E_a/k_B (K)	ν_∞ (GHz)
$La_{2-x}Sr_xNiO_4$	0.33	—	185(20)	—
$La_{1.8-x}Eu_{0.2}Sr_xCuO_4$	0.014	3.07(30)	44(4)	10.4(21)
	0.016	3.68(35)	25(2)	1.8(2)
	0.018	3.53(35)	22(3)	0.9(2)
	0.15	1.65(15)	39(3)	0.8(2)

fluctuations of the charge stripes with the observations. In the cuprate the activation energy of the stripe fluctuations is $\approx$30 K, which is six times smaller than in the nickelate. Transverse stripe fluctuations are microscopically realized by hopping processes of the doped holes. This result reflects the much stronger hole localization in the nickelates.

5. Electronic phase separation in $Pr_{2-x}Ce_xCuO_4$

If intrinsic charge inhomogeneities are truly universal in strongly doped 2D transition metal oxides they should not only be observed in hole doped cuprate systems but also in the electron doped analogues. The system $Pr_{2-x}Ce_xCuO_4$ is a prototype of an electron doped high-T_C cuprate [72–74]. It crystallizes in the tetragonal body centred T' structure which is a modification of the K_2NiF_4 structure (see figure 2). In this system the crystal field ground state of Pr^{3+} is a non-magnetic singlet with the first excited doublet at $\approx$210 K [75, 76], and Ce^{4+} ($4f^0$) acts as a non-magnetic electron donor [77]. Long-range AF order is observed in an extended Ce doping range $0 \leqslant x < 0.14$, whereas superconductivity is found for $0.14 < x < 0.18$ [73].

We examined polycrystalline samples of $Pr_{2-x}Ce_xCuO_4$ in the long-range AF ordered phase ($x = 0.05, 0.075, 0.10$ and 0.125) in ZF-μSR to identify inhomogeneous spin order [78]. Typical ZF frequency spectra are depicted in figure 20. In all samples a spontaneous muon spin precession was found below the respective Néel temperatures.

At high electron doping levels of $x = 0.10$ and 0.125, a significant non-precessing signal fraction of $\approx$40% remains even at the lowest temperatures studied. An inhomogeneous electronic ground state is found. Since the non-precessing signal fraction is also described by a static local field distribution with a finite line width—centred at zero frequency—we interpret it as a nanoscale coexistence of magnetic and non-magnetic domains where muons coming to rest in the non-magnetic volume fraction do experience stray fields from nearby magnetic domains. For lower doping ($x = 0.05$ and 0.075) this non-magnetic signal fraction of $\approx$40% is found only for $T > 40$ K. Below this temperature an additional increase of f_{mag} to 100% is observed.

X-ray powder diffractometry confirmed a structural phase purity better than 98%, and we associate our results with an intrinsic electronic phase separation into electron-rich and electron-poor domains. Susceptibility measurements above 3 K do not show a diamagnetic signal in these specimens [79]. This does not imply the absence of superconductivity. If the size of the nanoscale non-magnetic inclusions is much smaller than the magnetic penetration depth no Meissner screening is observed. Therefore the non-magnetic signal fraction persisting to low temperatures for $x = 0.10$ and 0.125 can also be associated with a superconducting volume fraction. The inhomogeneous magnetic ordering process observed for $x = 0.05$ and 0.075 may be explained by an electronic phase separation into two phases with slightly different electron doping levels giving rise to different Néel temperatures.
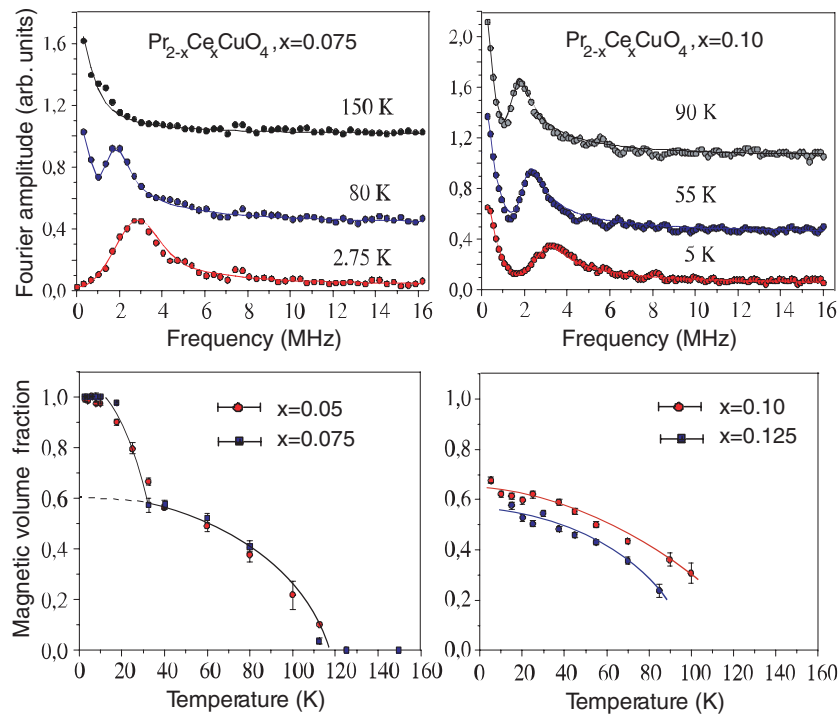
Figure 20. Upper panel: ZF-μSR frequency spectra of $Pr_{2-x}Ce_xCuO_4$ with $x = 0.075$ and 0.10 at different temperatures. Lower panel: temperature dependence of the magnetic volume fraction for $x = 0.05$, 0.075, 0.10 and 0.125 [81].

In a higher doped superconducting single crystal of $Pr_{2-x}Ce_xCuO_4$, recent μSR experiments by Sonier *et al* [80] also show a significant electronic relaxation of magnetic origin within the superconducting phase and support the existence of electronic phase inhomogeneity also for stronger electron doping. These results suggest that electronic charge inhomogeneity in regions with enhanced and reduced electron density is also an intrinsic property of the electron doped high-T_C cuprates.

6. Conclusions

In this paper we report μSR studies on 2D transition metal oxides to examine nanoscale inhomogeneous magnetic phases. In the nickelates spin stripe order is identified by two separated signals in the ZF-μSR frequency spectrum. In the cuprates a phase transition from superconductivity to magnetic stripe order in a wide charge carrier doping range x is controlled by small variations in the lattice structure. Our data suggest that the proximity of superconductivity and antiferromagnetism is important for a discussion of the electronic/magnetic properties of the cuprates in the entire superconducting region and not only in connection with the change from the long-range AF to the superconducting ground state at low charge carrier content x. The antiferromagnetism at high charge carrier doping is caused by the intrinsic tendency to create nanoscale charge inhomogeneities and the existence of lattice modulations of the same symmetry which act as pinning centres. The strong coupling of charge and spin degrees of freedom then promotes the formation of spin stripe ordered phases.

Acknowledgments

References

[1] Tranquada J M *et al* 1995 *Nature* **375** 561
[2] von Zimmermann M *et al* 1998 *Europhys. Lett.* **41** 629
[3] Lee S-H and Cheong S W 1997 *Phys. Rev. Lett.* **79** 2514
[4] Mori S *et al* 1998 *Nature* **392** 473
[5] Baberski O *et al* 1998 *Europhys. Lett.* **44** 335
[6] Hess C *et al* 1999 *Phys. Rev.* B **59** R10397
[7] Zaanen J and Gunnarsson O 1989 *Phys. Rev.* B **40** 7391
[8] Emery V *et al* 1999 *Proc. Natl Acad. Sci. USA* **96** 8814
[9] White S R *et al* 2002 *Phys. Rev.* B **65** 165122
[10] Carlson E W *et al* 2003 *The Physics of Conventional and Unconventional Superconductors* (Berlin: Springer)
[11] Kivelson S A *et al* 2003 *Rev. Mod. Phys.* **75** 1201
[12] Cheong S W *et al* 1991 *Phys. Rev. Lett.* **67** 1791
[13] Hayden S M *et al* 1992 *Phys. Rev. Lett.* **68** 1061
[14] Tranquada J M *et al* 2004 *Nature* **429** 534
[15] Furukawa Y *et al* 1999 *Phys. Rev.* B **59** 134155
[16] Curro N J *et al* 2000 *Phys. Rev. Lett.* **85** 642
[17] Teitel'baum G B *et al* 2000 *Phys. Rev.* B **63** 020507
[18] Hunt A *et al* 2001 *Phys. Rev.* B **64** 134525
[19] Abu-Shiekah I M *et al* 2001 *Phys. Rev. Lett.* **87** 237201-1
[20] Kataev V *et al* 1998 *Phys. Rev.* B **58** R11876
[21] Sulaiman S B *et al* 1994 *Phys. Rev.* B **49** 9879
[22] Suter H U *et al* 2003 *Physica* B **326** 329
[23] Amato A *et al* 1997 *Hyperfine Interact.* **104** 115
[24] Borsa F *et al* 1995 *Phys. Rev.* B **52** 7334
[25] Niedermayer C *et al* 1998 *Phys. Rev. Lett.* **80** 3843
[26] Sonier J E *et al* 2000 *Rev. Mod. Phys.* **72** 769
[27] Charalambous D *et al* 2002 *Phys. Rev.* B **66** 54506
[28] Gopalan P *et al* 1992 *Phys. Rev.* B **45** 249
[29] Wang P *et al* 1992 *Phys. Rev.* B **45** 5645
[30] Cava R J *et al* 1991 *Phys. Rev.* B **43** 1229
[31] Sachan V *et al* 1995 *Phys. Rev.* B **51** 12742
[32] Tranquada J M *et al* 1996 *Phys. Rev.* B **54** 12318
[33] Lee S H *et al* 1997 *Phys. Rev. Lett.* **79** 2514
[34] Martinez *et al* 1992 *J. Magn. Magn. Mater.* **104** 941
[35] Chow K *et al* 1996 *Phys. Rev.* B **53** R14725
[36] Fretoft T *et al* 1991 *Phys. Rev.* B **44** 5046
[37] Tranquada J M *et al* 1993 *Phys. Rev. Lett.* **70** 445
[38] Jestädt T *et al* 1999 *Phys. Rev.* B **59** 3775
[39] Klauss H-H *et al* 2001 *Hyperfine Interact.* **136** 711
[40] MacLaughlin D E *et al* 2001 *Phys. Rev. Lett.* **72** 760
[41] Furukawa Y and Wada S 1994 *J. Phys.: Condens. Matter* **6** 8023
[42] Yoshinari Y *et al* 2001 *Phys. Rev. Lett.* **82** 3536

[43] Slichter C P 1980 *Principles of Magnetic Resonance* (New York: Springer)
[44] Baabe D *et al* 2004 *Phys. Rev.* B **69** 134512
[45] Hayano R S *et al* 1979 *Phys. Rev.* B **20** 850
[46] Lee S H *et al* 2002 *Phys. Rev. Lett.* **88** 126401
[47] Tranquada J M 2004 *Neutron Scattering in Layered Copper-Oxide Superconductors* ed A Furrer (Dordrecht: Kluwer)
[48] Axe J D *et al* 1989 *Phys. Rev. Lett.* **62** 2751
[49] Luke J M *et al* 1991 *Physica* C **185** 185
[50] Kumagai K *et al* 1994 *Hyperfine Interact.* **86** 473
[51] Klauss H-H *et al* 2000 *Phys. Rev. Lett.* **85** 4590
[52] Lee S H *et al* 2001 *Phys. Rev.* B **63** R60405
[53] Hücker M *et al* 2004 in preparation
[54] Büchner B *et al* 1994 *Phys. Rev. Lett.* **73** 1841
[55] Wagener W *et al* 1997 *Phys. Rev.* B **55** R14761
[56] Wagener W *et al* 1997 *Hyperfine Interact.* **105** 107
[57] Luke G M *et al* 1997 *Hyperfine Interact.* **105** 113
[58] Lappas A *et al* 1997 *Hyperfine Interact.* **105** 101
[59] Nachumi B *et al* 1998 *Phys. Rev.* B **58** 8760
[60] Hücker M *et al* 1998 *J. Phys. Chem. Solids* **59** 1821
[61] Weidinger A *et al* 1989 *Phys. Rev. Lett.* **62** 102
[62] Tranquada J M *et al* 1996 *Phys. Rev.* B **54** 7489
[63] Wakimoto S *et al* 2000 *Phys. Rev.* B **61** 3699
[64] Matsuda M *et al* 2002 *Phys. Rev.* B **65** 134515
[65] van Duin C N A and Zaanen J 1998 *Phys. Rev. Lett.* **80** 1513
[66] Tallon J L and Loram J W 2001 *Physica* C **349** 53
[67] Jöstingmeier M *et al* 2002 *Preprint* cond-mat/0207528
[68] Klauss H-H *et al* 2002 *Physica* B **312** 71
[69] Hücker M *et al* 1999 *Phys. Rev.* B **59** R725
[70] Lappas A *et al* 2000 *J. Phys.: Condens. Matter* **12** 3401
[71] Kojima K M *et al* 2003 *Physica* B **326** 316
[72] Tokura Y *et al* 1989 *Nature* **337** 345
[73] Takagi H *et al* 1989 *Phys. Rev. Lett.* **62** 1197
[74] Luke G M *et al* 1990 *Phys. Rev.* B **42** 7981
[75] Matsuda M *et al* 1990 *Phys. Rev.* B **42** 10098
[76] Boothroyd A T *et al* 1992 *Phys. Rev.* B **45** 10075
[77] Alexander M *et al* 1991 *Phys. Rev.* B **43** 333
[78] Baabe D *et al* 2003 *Physica* B **326** 338
[79] Mennerich C *et al* 2004 *J. Magn. Magn. Mater.* **272** 162
[80] Sonier J *et al* 2003 *Phys. Rev. Lett.* **91** 147002
[81] Baabe D 2004 *PhD Thesis* in preparation